V European Conference on Computational Fluid Dynamics
ECCOMAS CFD 2010
J. C. F. Pereira and A. Sequeira (Eds)
Lisbon, Portugal,14-17 June 2010

DETERMINATION OF MODEL ORDER FOR INVERSE SCATTERING APPLICATIONS

Livia Cerullo*, Thomas Rylander† and Mats Viberg†

*,† Department of Signals and Systems
Chalmers University of Technology
SE-412 96 Göteborg
Sweden
e-mail: {cerullo,rylander,viberg}@chalmers.se

Key words: Inverse scattering, Maxwell's equations, Sensitivity analysis, Model order determination

Abstract. *We present and test a gradient based optimization algorithm for the solution of an inverse problem, where we solve Maxwell's equations in a 2D setting. We consider a model problem with six parallel-plate waveguides connected to a circular cavity, where the object under reconstruction resides inside the cavity. The goal function in the optimization problem is the misfit between the computed and measured scattering matrix averaged with respect to the waveguide ports and the frequency range used for the reconstruction. The inverse algorithm exploits the field solution of an adjoint problem to compute the gradient of the goal function. This approach yields a computational cost that is independent of the number of degrees of freedom used to describe the object under reconstruction. As a consequence of the reciprocity of Maxwell's equations, the value of the goal function and its gradient are relatively inexpensive to compute when the scattering matrix and the underlying field solutions are available. We use this reconstruction algorithm to study (i) the impact of the cell size on the reconstruction error, (ii) the reconstruction error that stems from an insufficient model order, and (iii) the influence of noise on the quality of the reconstructions.*

1 INTRODUCTION

Inverse problems arise in many applications: non-destructive testing;[1] non-invasive detection of tumors;[2] monitoring of industrial processes;[3] and subsurface sensing.[4] Electromagnetic waves in the microwave frequency range are good for many of these applications. In medical applications, it is advantageous to avoid X-rays since they are ionizing and, therefore, microwave tomography is considered a good alternative. In some cases, impedance tomography is a possible alternative, but such an approach yields a lower resolution for the reconstructions as compared to microwaves.

For the reconstruction of the material parameters in an inhomogeneous region, it is advantageous to exploit the finite element method (FEM)[5] or similar techniques[6] to solve Maxwell's equations. For such situations, it is common to use at least one material parameter degree of freedom for each computational cell, which yields a large number of material parameters to determine by means of the reconstruction algorithm that often must exploit regularization.[7] For example, the finite-difference time-domain (FDTD) scheme has been used for inverse problems in such a setting.[8,9] Another alternative[2] is to use an underlying model for the material description, where the model features a set of basis functions and corresponding coefficients that are determined by the reconstruction algorithm. This approach has some distinct advantages: (i) it is feasible to incorporate a priori information about the material distribution subject to reconstruction; (ii) the number of degrees of freedom in the reconstruction problem is significantly reduced; (iii) the resolution for the reconstructed material parameter is decoupled from the cell size used for the solution of Maxwell's equations; and (iv) the sensitivity to measurement noise can be controlled and mitigated by reducing the flexibility of the material parameterization for parts of the parameter space that are not necessary for a successful reconstruction. However, it is necessary to choose a parameterization with a model order that is sufficiently high to capture the spatial variations of the material distribution subject to reconstruction, but not too high since that results in a flexibility of the parameterized material which may approximate measurement noise instead of improving the reconstruction.

In this article, we present an inverse scattering algorithm for Maxwell's equations applied to 2D problems. Our model problem consists of a number of parallel-plate waveguides connected to a circular cavity, which contains the object subject to reconstruction. The reconstruction algorithm is formulated as a minimization problem with a goal function that features the misfit of the computed and measured scattering matrix and, here, we average this misfit with respect to the waveguide ports and the frequency. Based on the continuum form of Maxwell's equations, we formulate the sensitivity[10] of the scattering matrix (and the goal function) with respect to changes in the permittivity in the cavity by a combination of the continuum field solution to (i) the original field problem and (ii) an adjoint field problem. Here, the adjoint field problems are identical to the original field problems, which is a consequence of the reciprocity of Maxwell's equations. Thus, we get the value of the goal function and its gradient provided that we have computed the field solutions that are necessary for the evaluation of the scattering matrix. The computational cost for the gradient of the goal function is independent of the model order that is used to express the permittivity distribution subject to reconstruction. In addition, our continuum formulation decouples the field solver from the optimization method, which allows for good flexibility in the choice of the field solver.

Here, we exploit this computational environment to investigate the effect on the reconstructed object due to different types of errors: (i) discretization errors in the FEM; (ii) errors due to a material parameterization of finite model order; and (iii) errors due to measurements contaminated by noise. In order to perform these studies, we compute accurate reference solutions by extrapolation to zero cell size.

2 BOUNDARY VALUE PROBLEM

Here, we consider a model problem in 2D and the geometry is shown in Fig. 1. The region subject to reconstruction is located in a circular cavity of radius r_0, and in Fig. 1 this region is described by $x^2 + y^2 < r_0^2$. The cavity is equipped with P parallel-plate waveguides connected to and uniformly distributed around its perimeter. The cavity and waveguide boundaries are modeled as a perfect electric conductor (PEC).

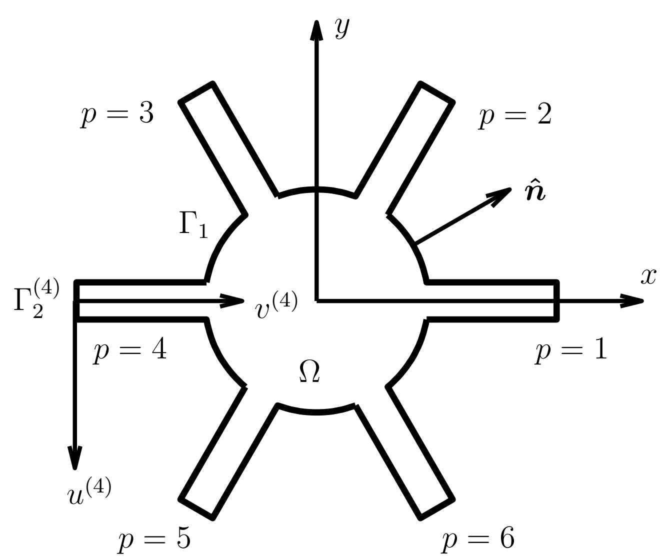

Figure 1: Geometry for the inverse scattering model problem: circular cavity with the region subject to reconstruction; P parallel-plate waveguides connected to the perimeter of the circular cavity; and a local coordinate system $(u^{(4)}, v^{(4)})$ used to describe the Robin boundary condition at $\Gamma_2^{(4)}$ associated with the port $p = 4$.

Given this geometry, we consider the case when the magnetic field $\boldsymbol{H}$ is transverse to the cylinder axis and it satisfies the boundary value problem

$$\nabla \times (\epsilon^{-1} \nabla \times \boldsymbol{H}) - \omega^2 \mu_0 \boldsymbol{H} = \boldsymbol{0} \qquad \text{on } \Omega \tag{1}$$

$$\hat{\boldsymbol{n}} \times (\epsilon^{-1} \nabla \times \boldsymbol{H}) = \boldsymbol{0} \qquad \text{on } \Gamma_1 \tag{2}$$

$$\hat{\boldsymbol{n}} \times (\epsilon^{-1} \nabla \times \boldsymbol{H}) + \gamma^{(p)}\, \hat{\boldsymbol{n}} \times (\hat{\boldsymbol{n}} \times \boldsymbol{H}) = \boldsymbol{Q}^{(p)} \qquad \text{on } \Gamma_2^{(p)} \text{ for } p = 1, \ldots, P \tag{3}$$

Here, $\epsilon = \epsilon_0 \epsilon_{\mathrm{r}}$ is the permittivity and $\hat{\boldsymbol{n}}$ is the unit normal vector to the boundary Γ, where Γ is the union of the PEC boundary Γ_1 and the waveguide ports $\Gamma_2^{(p)}$ for $p = 1, \ldots, P$. The relative permittivity ϵ_{r} is unity in the parallel-plate waveguides. Inside the circular cavity, the relative permittivity $\epsilon_{\mathrm{r}} = \epsilon_{\mathrm{r}}(x, y) \geq 1$ and it is subject to reconstruction. Furthermore, the Robin boundary condition (3) at port p allows for an incident field $\boldsymbol{H}_p^+$ and we use

$$\gamma^{(p)} = j\omega Z_{10} \tag{4}$$

$$\boldsymbol{Q}^{(p)} = 2j\omega Z_{10} \hat{\boldsymbol{n}} \times \hat{\boldsymbol{n}} \times \boldsymbol{H}_p^+ \tag{5}$$

Here, the wave impedance is $Z_{10} = \omega\mu_0 / k_v$, the wave number $k_v = \sqrt{(\omega/c_0)^2 - (\pi/w)^2}$, the waveguide width w and the speed of light $c_0 = 1/\sqrt{\epsilon_0 \mu_0}$. We use operating frequencies that only allow the fundamental mode to propagate in the waveguides, i.e. $1 < 2fw/c_0 < 2$. Thus, we let the incident field $\boldsymbol{H}_p^+$ be the fundamental waveguide mode with the amplitude E_{0p}^+/Z_{10}, where E_{0p}^+ is the amplitude of the corresponding electric field. The amplitude E_{0p}^+ is a natural quantity to use for the definition of the scattering parameters that are used later in this paper.

Furthermore, the Robin boundary condition (3) absorbs the reflected field $\boldsymbol{H}_p^-$ with the unknown amplitude E_{0p}^-/Z_{10}, where the corresponding electric field amplitude E_{0p}^- is used again for the purpose of the upcoming definition of the scattering parameters. In the vicinity of the ports, the fields are consequently a superposition of the incident and reflected fundamental waveguide modes given by

$$\boldsymbol{H}_p^{\pm} = \frac{E_{0p}^{\pm}}{Z_{10}} \left[\pm\, \hat{\boldsymbol{u}}^{(p)} \cos\left(\frac{\pi u^{(p)}}{w}\right) + \hat{\boldsymbol{v}}^{(p)} j \frac{\pi}{k_v w} \sin\left(\frac{\pi u^{(p)}}{w}\right) \right] e^{\mp j k_v v^{(p)}}. \tag{6}$$

where $\hat{\boldsymbol{u}}^{(p)}$ and $\hat{\boldsymbol{v}}^{(p)}$ denote the unit vectors of a local coordinate system $(u^{(p)}, v^{(p)})$ associated with the port p according to Fig. 1. (In the numerical tests that follow, we have verified that the waveguide ports are sufficiently far from the waveguide apertures, which implies that higher order modes are negligible at the waveguide ports.)

2.1 Finite element method

We exploit the FEM[5] to solve the boundary value problem described above. The weak form states: find $\boldsymbol{H} \in H(\mathrm{curl}; \Omega)$ such that

$$a(\boldsymbol{w}, \boldsymbol{H}) = b(\boldsymbol{w}) \tag{7}$$

for all $\boldsymbol{w} \in H(\text{curl};\Omega)$. Here, the function space $H(\text{curl};\Omega)$ is defined by

$$H(\text{curl};\Omega) = \{\boldsymbol{w} : \boldsymbol{w} \in L_2(\Omega) \text{ and } \nabla \times \boldsymbol{w} \in L_2(\Omega)\} \tag{8}$$

and

$$a(\boldsymbol{u},\boldsymbol{v}) = \int_\Omega [\epsilon^{-1}(\nabla \times \boldsymbol{u}) \cdot (\nabla \times \boldsymbol{v}) - \omega^2 \mu_0 \, \boldsymbol{u} \cdot \boldsymbol{v}] d\Omega \tag{9}$$
$$+ \sum_{p=1}^{P} \gamma^{(p)} \int_{\Gamma_2^{(p)}} (\hat{\boldsymbol{n}} \times \boldsymbol{u}) \cdot (\hat{\boldsymbol{n}} \times \boldsymbol{v}) d\Gamma$$

$$b(\boldsymbol{u}) = \sum_{p=1}^{P} b_p(\boldsymbol{u}) = -\sum_{p=1}^{P} \int_{\Gamma_2^{(p)}} \boldsymbol{u} \cdot \boldsymbol{Q}^{(p)} \, d\Gamma \tag{10}$$

We triangulate Ω by means of the Delaunay algorithm implemented in the software Triangle.[11] On this triangulation, we expand the magnetic field in terms of the lowest-order curl-conforming vector elements[12] that are tailor-made for approximations in $H(\text{curl};\Omega)$. (See the book[5] by Jin for explicit expressions of the basis functions for curl-conforming vector elements on triangles and engineering application examples.)

3 SENSITIVITY ANALYSIS

The scattering parameters[13] are defined as

$$S_{pq} = \left. \frac{V_{0p}^-}{V_{0q}^+} \right|_{V_{0k}^+=0 \; for \; k \neq q} \tag{11}$$

where V_{0q}^+ is the voltage amplitude of the incident wave at port q and V_{0p}^- is the voltage amplitude of the reflected wave at port p. Here, the voltages $V_{0p}^\pm$ are directly proportional to $E_{0p}^\pm$, where the proportionality constant is identical for all ports.

Thus, the scattering parameters can be expressed as the ratio between the incident and reflected field amplitudes

$$S_{pq} = \frac{E_{0p}^-}{E_{0q}^+} = \frac{E_{0p}^+}{E_{0q}^+} e^{-2jk_v v^{(p)}} - \frac{\mu_0}{jk_v w E_{0p}^+ E_{0q}^+} b_p(\boldsymbol{H}) \tag{12}$$

3.1 Sensitivity derivation

Given a perturbation $\delta\epsilon$ of the original permittivity ϵ inside the cavity, the new material distribution $\epsilon + \delta\epsilon$ yields a perturbation $\delta\boldsymbol{H}$ of the original magnetic field $\boldsymbol{H}$. Thus, we have that the first-order variation of the scattering parameters (12) due to an infinitesimal change $\delta\epsilon$ in the permittivity distribution can be expressed as

$$\delta S_{pq} = \zeta b_p(\delta \boldsymbol{H}) \tag{13}$$

where $\zeta = -\mu_0 (j k_v w E_{0p}^{+} E_{0q}^{+})^{-1}$.

Now, we choose the adjoint problem

$$a(\delta \boldsymbol{H}, \boldsymbol{F}) = b_p(\delta \boldsymbol{H}) \tag{14}$$

where $\boldsymbol{F}$ is the adjoint solution. The solution of the adjoint problem allows us to express the variation of the scattering parameters as

$$\delta S_{pq} = \zeta a(\delta \boldsymbol{H}, \boldsymbol{F}) = \zeta a(\boldsymbol{F}, \delta \boldsymbol{H}) \tag{15}$$

where we have exploited that the bilinear form (9) is self-adjoint.

Next, we consider the perturbed problem

$$(a + \delta a)(\boldsymbol{w}, \boldsymbol{H} + \delta \boldsymbol{H}) = b(\boldsymbol{w}) \tag{16}$$

and the terms that involve the first-order variation yield $a(\boldsymbol{w}, \delta \boldsymbol{H}) + \delta a(\boldsymbol{w}, \boldsymbol{H}) = 0$, where we exploit that $a(\boldsymbol{w}, \boldsymbol{H}) = b(\boldsymbol{w})$ and neglect the higher-order terms.

Thus, we can express the first-order variation (15) of the scattering parameters as

$$\delta S_{pq} = -\zeta \delta a(\boldsymbol{F}, \boldsymbol{H}) \tag{17}$$

where we have[14]

$$\delta a(\boldsymbol{F}, \boldsymbol{H}) = -\int_{\Omega} \frac{\delta \epsilon}{\epsilon^2} (\nabla \times \boldsymbol{F}) \cdot (\nabla \times \boldsymbol{H}) d\Omega \tag{18}$$

Finally, the sensitivity of the scattering parameters S_{pq} with respect to changes in the permittivity ϵ is given by

$$\delta S_{pq} = -\frac{\mu_0}{j k_v w E_{p,\mathrm{adj}}^{+} E_{q,\mathrm{orig}}^{+}} \int_{\Omega} \frac{\delta \epsilon}{\epsilon^2} (\nabla \times \boldsymbol{H}_{\mathrm{adj}}) \cdot (\nabla \times \boldsymbol{H}_{\mathrm{orig}}) d\Omega \tag{19}$$

Here, the original field problem yields the field solution $\boldsymbol{H}_{\mathrm{orig}}$, where $E_{q,\mathrm{orig}}^{+}$ is the amplitude of the incident wave on port q. Similarly, the adjoint field solution $\boldsymbol{H}_{\mathrm{adj}}$ is computed with an incident wave on port p where the amplitude is $E_{p,\mathrm{adj}}^{+}$.

We emphasize that the adjoint problem is identical to the original problem due to the reciprocity of Maxwell's equations and, consequently, the computational cost for the sensitivities δS_{pq} is relatively small given that the scattering matrix and the underlying field solutions are already computed. The technique presented here is similar to the approach used for reduction of the radar cross section,[14] optimization of microwave devices[15] and shape reconstruction of metallic surfaces.[16]

4 RECONSTRUCTION ALGORITHM

Given the measured scattering parameters S_{pq}^{M}, we attempt to reconstruct the permittivity $\epsilon(\boldsymbol{r})$ inside the cavity, i.e. in the region $x^2 + y^2 < r_0^2$. Thus, we parameterize the permittivity $\epsilon = \epsilon(\boldsymbol{r}; a_1, \ldots, a_M)$ in terms of a series with unknown coefficients a_k and some appropriate basis functions $\varphi_k(\boldsymbol{r})$. The material parameters a_k are collected in a vector $\mathbf{a}$.

Thus, we attempt to reconstruct the permittivity profile (described by the material parameter vector $\mathbf{a}$) by minimizing the goal function

$$g(\mathbf{a}) = \left[\frac{1}{P^2} \sum_{p=1}^{P} \sum_{q=1}^{P} \frac{1}{f_{\mathrm{U}} - f_{\mathrm{L}}} \int_{f_{\mathrm{L}}}^{f_{\mathrm{U}}} |S_{pq}^{\mathrm{C}}(f; \mathbf{a}) - S_{pq}^{\mathrm{M}}(f)|^2 df \right]^{\frac{1}{2}} \tag{20}$$

In practice, we exploit the `SNOPT` algorithm implemented in `TOMLAB`.[17] Thus, we solve the minimization problem

$$\begin{aligned} \mathbf{a}^* = &\arg \min_{\mathbf{a}} g(\mathbf{a}) \\ &\text{s.t. } \epsilon(\boldsymbol{r}; \mathbf{a}) \geq \epsilon_0 \ \forall \boldsymbol{r} \in \Omega \end{aligned} \tag{21}$$

4.1 Parameterization of the permittivity

In this article, we consider a model problem with an axisymmetric permittivity profile, which implies that the permittivity is only a function of the distance to the center of the circular cavity, i.e. $\epsilon = \epsilon(r)$. We parameterize the relative permittivity ϵ_{r} profile by means of a Bézier curve with M degrees of freedom, i.e.,

$$\epsilon_{\mathrm{r}}(r) = \sum_{k=0}^{M-1} a_{k+1} B_k^{M-1}\left(\frac{r}{r_0}\right) \tag{22}$$

Here, $B_k^m(t)$ is the k-th Bernstein polynomial of degree m and it is given by

$$B_k^m(t) = \binom{m}{k} t^k (1-t)^{m-k} \qquad \text{for } k = 0, \ldots, m \tag{23}$$

where $t \in [0, 1]$. The Bézier curve is located within the convex hull of its control points and, consequently, it is feasible to guarantee that the relative permittivity satisfies the condition $\epsilon_{\mathrm{r}}(r) \geq 1$ for $0 \leq r \leq r_0$ by imposing the requirement $a_k \geq 1$ for $k = 1, \ldots, M$.

4.2 Measurements with noise

In an experimental setup, the measured response S_{pq}^{M} is composed of the exact response S_{pq}^0 and an unwanted disturbance S_{pq}^{dist}, i.e. $S_{pq}^{\mathrm{M}} = S_{pq}^0 + S_{pq}^{\mathrm{dist}}$. Here, we consider the case when S_{pq}^{dist} stems from measurement noise and, in particular, we are interested in the situation where the disturbance is small, i.e. $|S_{pq}^{\mathrm{dist}}| \ll |S_{pq}^0|$.

For such a situation, we exploit the linearization

$$S_{pq}^{\mathrm{C}}(f;\mathbf{a}^*+\delta\mathbf{a}) = S_{pq}^{\mathrm{C}}(f;\mathbf{a}^*) + \left[\nabla_{\mathbf{a}} S_{pq}^{\mathrm{C}}(f;\mathbf{a})|_{\mathbf{a}=\mathbf{a}^*}\right]^{\mathrm{T}} \delta\mathbf{a} + \ldots \tag{24}$$

of the computed scattering matrix with respect to the parameter vector $\mathbf{a}$, where we neglect the higher-order terms in the series expansion. Here, $\mathbf{a}^*$ is the solution to the non-linear optimization problem (21) for an idealized situation where there is no disturbance in the signal S_{pq}^{M}, i.e. $S_{pq}^{\mathrm{M}} = S_{pq}^{0}$. This is of course unrealistic in an experiment but, in this article, we generate such a response by means of computation since it gives us the possibility to study the influence of measurement noise on the reconstructed profiles.

Next, we consider the misfit $|S_{pq}^{\mathrm{C}}(f;\mathbf{a}^*+\delta\mathbf{a}) - S_{pq}^{\mathrm{M}}(f)|$ that features in the goal function (20) and, in particular, we express this misfit as

$$\begin{aligned} |S_{pq}^{\mathrm{C}}(f;\mathbf{a}^*+\delta\mathbf{a}) - S_{pq}^{\mathrm{M}}(f)| &= \left| S_{pq}^{\mathrm{C}}(f;\mathbf{a}^*) + \left[\nabla_{\mathbf{a}} S_{pq}^{\mathrm{C}}(f;\mathbf{a})|_{\mathbf{a}=\mathbf{a}^*}\right]^{\mathrm{T}} \delta\mathbf{a} - (S_{pq}^{0}(f) + S_{pq}^{\mathrm{dist}}(f)) \right| \\ &= \left| \left(S_{pq}^{\mathrm{C}}(f;\mathbf{a}^*) - S_{pq}^{0}(f) \right) + \left(\left[\nabla_{\mathbf{a}} S_{pq}^{\mathrm{C}}(f;\mathbf{a})|_{\mathbf{a}=\mathbf{a}^*}\right]^{\mathrm{T}} \delta\mathbf{a} - S_{pq}^{\mathrm{dist}}(f) \right) \right| \end{aligned}$$

Within the region of validity for the linearization (24), we can consequently compute the deviation $\delta\mathbf{a}$ from the optimum $\mathbf{a}^*$ due to the noise S_{pq}^{dist} from the overdetermined system of linear equations

$$\begin{pmatrix} \Re\{\mathbf{G}\} \\ \Im\{\mathbf{G}\} \end{pmatrix} \delta\mathbf{a} = \begin{pmatrix} \Re\{\mathbf{s}\} \\ \Im\{\mathbf{s}\} \end{pmatrix} \tag{25}$$

where

$$G_{ij} = \left. \frac{\partial S_{pq}^{\mathrm{C}}(f_n;\mathbf{a})}{\partial a_j} \right|_{\mathbf{a}=\mathbf{a}^*} \tag{26}$$

$$s_i = S_{pq}^{\mathrm{dist}}(f_n) \tag{27}$$

with the row index $i = 1, \ldots, P^2 N$ that corresponds to a sequential numbering of the triplets (p, q, n). Here, we consider all combinations of the port indices $p = 1, \ldots, P$ and $q = 1, \ldots, P$. Further, we use the index $n = 1, \ldots, N$ for the discrete frequency points $f_n = (f_{\mathrm{U}} - f_{\mathrm{L}})(n-1)/(N-1) + f_{\mathrm{L}}$. (The column index $j = 1, \ldots, M$ corresponds to the coefficient a_j in the parameterization.) Equation (25) only involves real-valued quantities, where the real part is denoted $\Re\{\cdot\}$ and the imaginary part is denoted $\Im\{\cdot\}$.

Given the small disturbance S_{pq}^{dist}, the overdetermined system of linear equations (25) yields a rather good approximation $\hat{\mathbf{a}} = \mathbf{a}^* + \delta\mathbf{a}$ to the solution of the non-linear optimization problem (21) with the measurement $S_{pq}^{\mathrm{M}} = S_{pq}^{0} + S_{pq}^{\mathrm{dist}}$. Thus, we can generate statistics for the case when S_{pq}^{dist} is a complex random variable with zero mean and sufficiently small standard deviation, which is feasible given a relatively small computational cost.

5 RESULTS

The geometry of the model problem is shown in Fig. 1. In the following, we use a circular cavity of radius $r_0 = 0.1$ m and six parallel-plate waveguides of width $w = 0.04$ m and length 0.14 m. For this setting, we consider the reconstruction of two different permittivity profiles:

- **Case A**: As a first test case, the permittivity $\epsilon_{\mathrm{r}}^{\mathrm{A}}(r)$ is created by means of the parameterization (22) with $M = 6$ and

$$\mathbf{a}^* = [2, 2, 1.1, 1.2, 1.7, 1.7].$$

  This gives a permittivity profile $\epsilon_{\mathrm{r}}^{\mathrm{A}}(r)$ that the reconstruction algorithm can express exactly since it is also based on the Bézier curve parameterization (22). We find this type of permittivity profile useful for testing purposes.

- **Case B**: The smooth permittivity profile $\epsilon_{\mathrm{r}}^{\mathrm{B}}(r)$ is expressed as

$$\begin{aligned}\epsilon_{\mathrm{r}}^{\mathrm{B}}(r) = 2 - 0.3 &\left(\mathrm{erf}\left(\frac{r - r_{\mathrm{m1}}}{\delta r_1}\right) - \mathrm{erf}\left(\frac{-r_{\mathrm{m1}}}{\delta r_1}\right)\right) \\ + 0.1 &\left(\mathrm{erf}\left(\frac{r - r_{\mathrm{m2}}}{\delta r_2}\right) - \mathrm{erf}\left(\frac{-r_{\mathrm{m2}}}{\delta r_2}\right)\right)\end{aligned} \tag{28}$$

  which cannot be represented exactly by the parameterization (22). Here, we use $r_{\mathrm{m1}} = 0.02$ m, $\delta r_1 = 0.004$ m, $r_{\mathrm{m2}} = 0.06$ m and $\delta r_2 = 0.008$ m.

The permittivity profiles for the two cases are shown in Fig. 2. Given these two permittivity profiles on closed form, we exploit the FEM to compute the 6×6 scattering matrix for six uniformly distributed frequency points f_n in the interval from $f_{\mathrm{L}} = 3.8$ GHz to $f_{\mathrm{U}} = 4.2$ GHz, i.e. $f_n = (f_{\mathrm{U}} - f_{\mathrm{L}})(n-1)/(N-1) + f_{\mathrm{L}}$ where $n = 1, \ldots, N$ and $N = 6$. For each frequency point, we perform a convergence study with hierarchical mesh refinement for $\lambda_{\mathrm{min}}/h = 5$, 10, 15, 20, 30, 45 and 60 points per wavelength, where h denotes the cell size and λ_{min} is the free-space wavelength at the highest frequency f_{U}. The computed results are extrapolated to zero cell size and we use these results as an approximation for S_{pq}^0.

5.1 Case A – reconstruction subject to discretization errors

Here, we consider the error in the reconstruction $\epsilon_{\mathrm{r}}(r; \mathbf{a}^*)$ of the permittivity profile $\epsilon_{\mathrm{r}}^{\mathrm{A}}$ due to discretization errors in the FEM solution of Maxwell's equations for our model problem. In particular, we are interested in the relative error $\mathcal{E}_{\epsilon_{\mathrm{r}}^{\mathrm{A}}} = ||\epsilon_{\mathrm{r}}(r; \mathbf{a}^*) - \epsilon_{\mathrm{r}}^{\mathrm{A}}(r)||_2 / ||\epsilon_{\mathrm{r}}^{\mathrm{A}}(r)||_2$ as a function of the number of points per wavelength λ_{min}/h. Here, we use $M = 6$ degrees of freedom for the parameterization of the permittivity and, consequently, the parameterization of the relative permittivity can exactly represent the

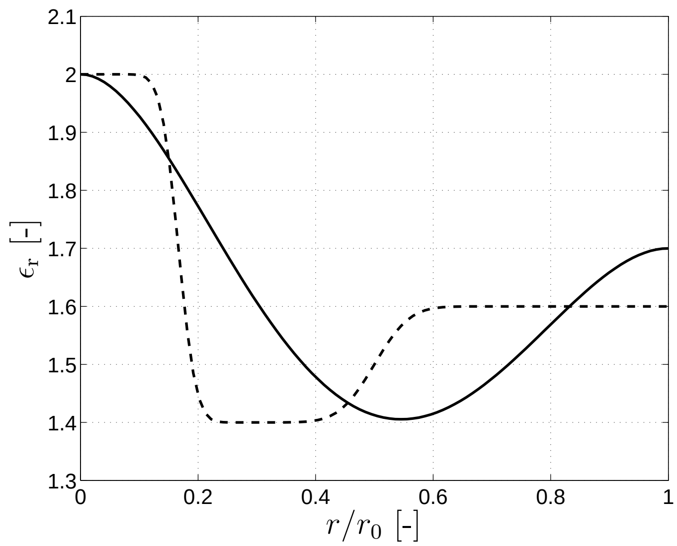

Figure 2: Exact permittivity profiles subject to reconstruction: ϵ_r^A – solid curve; and ϵ_r^B – dashed curve.

permittivity ϵ_r^A subject to reconstruction. We use $S_{pq}^M = S_{pq}^0$ and, thus, the reconstruction error $\mathcal{E}_{\epsilon_r^A}$ is due to a combination of (i) the FEM discretization errors and (ii) errors associated with the non-linear optimization problem (21) and its termination criterion. The optimized parameter vector $\mathbf{a}^*$ is computed by `TOMLAB`,[17] where we started with an initial parameter vector $\mathbf{a}$ close to the optimum and terminated the reconstruction after 70 major iterations. We find that the error in the reconstruction scales as $h^{4/3}$, which is also the convergence rate for the scattering parameters due to the sharp corners where the parallel-plate waveguides are connected to the cavity.[18] We perform the convergence study for three different resolutions: $\lambda_{\min}/h = 20$ yields $\mathcal{E}_{\epsilon_r^A} = 1.8\%$; $\lambda_{\min}/h = 40$ yields $\mathcal{E}_{\epsilon_r^A} = 0.70\%$; and $\lambda_{\min}/h = 80$ yields $\mathcal{E}_{\epsilon_r^A} = 0.25\%$. Thus, we achieve an error in the reconstruction that is about 1% for $\lambda_{\min}/h = 30$ and we use this resolution to compute S_{pq}^C for all the reconstruction tests that follow.

5.2 Case A – reconstruction subject to modeling errors

Next, we attempt to reconstruct the permittivity profile ϵ_r^A when it is represented by the parameterization (22) for different number of degrees of freedom M. Again, we exclude measurement noise and, consequently, we use $S_{pq}^M = S_{pq}^0$. Figure 3 shows the reconstructed relative permittivity $\epsilon_r(r; \mathbf{a}^*)$ for different number of degrees of freedom: $M = 5$ – thin solid curve; $M = 4$ – dashed curve; $M = 3$ – dash-dotted curve; and $M = 2$ – dotted curve. In order to facilitate comparisons, we also include $\epsilon_r^A(r)$ in Fig. 3 and it is shown by the thick solid curve. It is clear that the model error is large for low values of M and that it is reduced as M approaches the value used to generate ϵ_r^A.

Figure 4 shows the relative error $\mathcal{E}_{\epsilon_r^A} = ||\epsilon_r(r; \mathbf{a}^*) - \epsilon_r^A(r)||_2 / ||\epsilon_r^A(r)||_2$ in the reconstructed permittivity profile with respect to the number of degrees of freedom M that are

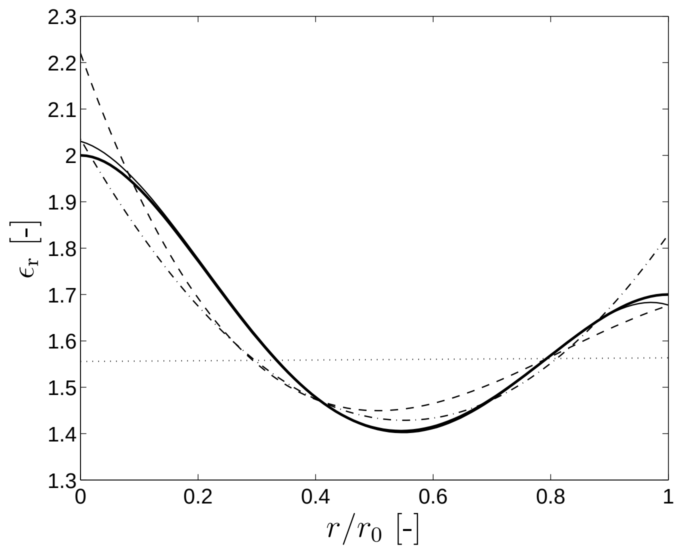

Figure 3: Reconstructed permittivity $\epsilon_r(r; \mathbf{a}^*)$ as a function of radius: $M = 5$ – thin solid curve; $M = 4$ – dashed curve; $M = 3$ – dash-dotted curve; and $M = 2$ – dotted curve. The true permittivity ϵ_r^A is shown by the thick solid curve to facilitate comparisons.

used in the reconstruction. Since ϵ_r^A is generated with $M = 6$, we expect reconstructions with $M \geq 6$ to yield a small reconstruction error and this is clearly seen in Fig. 4. On the contrary, $M < 6$ may yield a large reconstruction error due to the inability of the parameterization to approximate ϵ_r^A and, in particular, we notice that the reconstruction error is significantly larger than the error due to the FEM discretization for $M \leq 4$.

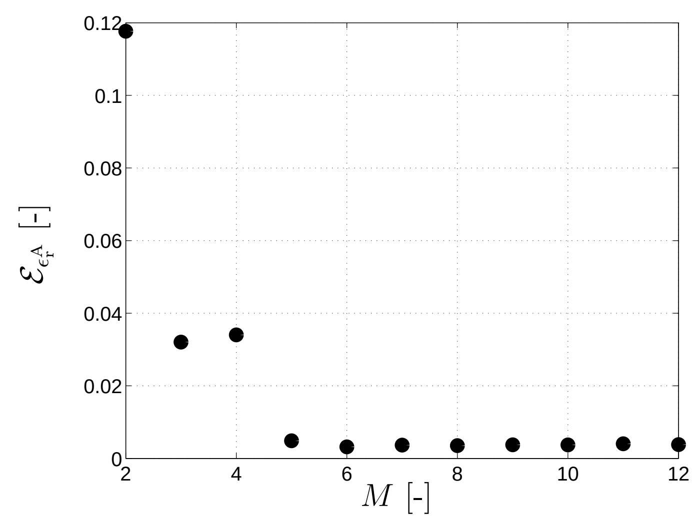

Figure 4: Reconstruction error as a function of the number of degrees of freedom M in the parameterization of the relative permittivity.

5.3 Case A – reconstruction subject to model errors and noise

Next, we consider the reconstruction quality as noise is added to S^0_{pq}, i.e. the reconstruction is based on $S^{\mathrm{M}}_{pq} = S^0_{pq} + S^{\mathrm{dist}}_{pq}$ where S^{dist}_{pq} is an independent complex Gaussian random variable with zero mean and the standard deviation σ. Our objective is to find the standard deviation in the reconstructed permittivity profile according to the procedure presented in Sec. 4.2, which is related to the work by Ye et al.[19,20] Figure 5 shows the relative permittivity ϵ_{r} as a function of the radial coordinate: thick solid curves – the permittivity $\epsilon^{\mathrm{A}}_{\mathrm{r}}$ subject to reconstruction; thin solid curves – the expected value $m_{\epsilon_{\mathrm{r}}}(r) = E[\epsilon_{\mathrm{r}}(r;\hat{\mathbf{a}})]$; and thin dashed curves – bounds for the region $m_{\epsilon_{\mathrm{r}}} - \tilde{\sigma}_{\epsilon_{\mathrm{r}}} < \epsilon_{\mathrm{r}} < m_{\epsilon_{\mathrm{r}}} + \tilde{\sigma}_{\epsilon_{\mathrm{r}}}$ with $\tilde{\sigma}_{\epsilon_{\mathrm{r}}}(r) = 0.1\sigma_{\epsilon_{\mathrm{r}}}(r)/\max_r \sigma_{\epsilon_{\mathrm{r}}}(r)$ and the standard deviation for the relative permittivity $\epsilon_{\mathrm{r}}(r;\hat{\mathbf{a}})$ denoted by $\sigma_{\epsilon_{\mathrm{r}}}(r)$. Consequently, the thin dashed curves in Fig. 5 indicate the variation of the standard deviation $\sigma_{\epsilon_{\mathrm{r}}}(r)$ with respect to the radial coordinate. In Fig. 5, the different subplots correspond to different number of degrees of freedom in the parameterization of the relative permittivity ϵ_{r}: $M = 2$ – top-left; $M = 3$ – top-right; $M = 4$ – middle-left; $M = 5$ – middle-right; $M = 6$ – bottom-left; and $M = 7$ – bottom-right. (The corresponding figures for $8 \leq M \leq 12$ are rather similar to $M = 7$ and, therefore, these are not included here.)

Figure 6 shows the standard deviation $\sigma_{\epsilon_{\mathrm{r}}}(r)$ for the relative permittivity: $M = 4$ – solid curve; $M = 6$ – dashed curve; $M = 9$ – dash-dotted curve; and $M = 12$ – dotted curve. The largest standard deviation occurs for $M = 12$ at $r = 0$ and, in Fig. 6, its value is 0.01 which occurs for a signal-to-noise ratio (SNR) of about 104 dB. Here and in the following, the SNR is computed in relation to $|S_{pq}|$ of unity magnitude.

For different values of M, Tab. 1 gives the SNR that is required for a maximum standard deviation of 0.05 in the relative permittivity. It is noticed that as the number of the degrees of freedom M for the parameterization of the relative permittivity is increased, it is necessary to perform more accurate measurements in order to maintain a constant maximum reconstruction error. Further, Tab. 1 gives the relative error $\mathcal{E}_{\epsilon^{\mathrm{A}}_{\mathrm{r}}} = ||\epsilon_{\mathrm{r}}(r;\mathbf{a}^*) - \epsilon^{\mathrm{A}}_{\mathrm{r}}(r)||_2/||\epsilon^{\mathrm{A}}_{\mathrm{r}}(r)||_2$ in the L_2-norm for the different values of M. Given these results, the relative error $\mathcal{E}_{\epsilon^{\mathrm{A}}_{\mathrm{r}}}$ decreases for $M \leq 6$ as M is increased and then remains constant under the assumption that the SNR is increased to a sufficiently high level for each individual M. In a practical situation, the SNR may be limited by the measurement setup and, consequently, this also imposes an upper bound on the highest possible model order without degradation in the reconstructions due to noise in the measurement.

5.4 Case B

Finally, we attempt to reconstruct the permittivity profile $\epsilon^{\mathrm{B}}_{\mathrm{r}}$, which cannot be expressed exactly by the Bézier curve parameterization (22). Figure 7 shows the reconstructions for three different number of parameters: $M = 10$ – dash-dotted curve; $M = 15$ – dashed curve; and $M = 20$ – solid curve. Here, it should be noticed that we use a global polynomial for the entire domain subject to reconstruction, i.e. $0 \leq r \leq r_0$. This

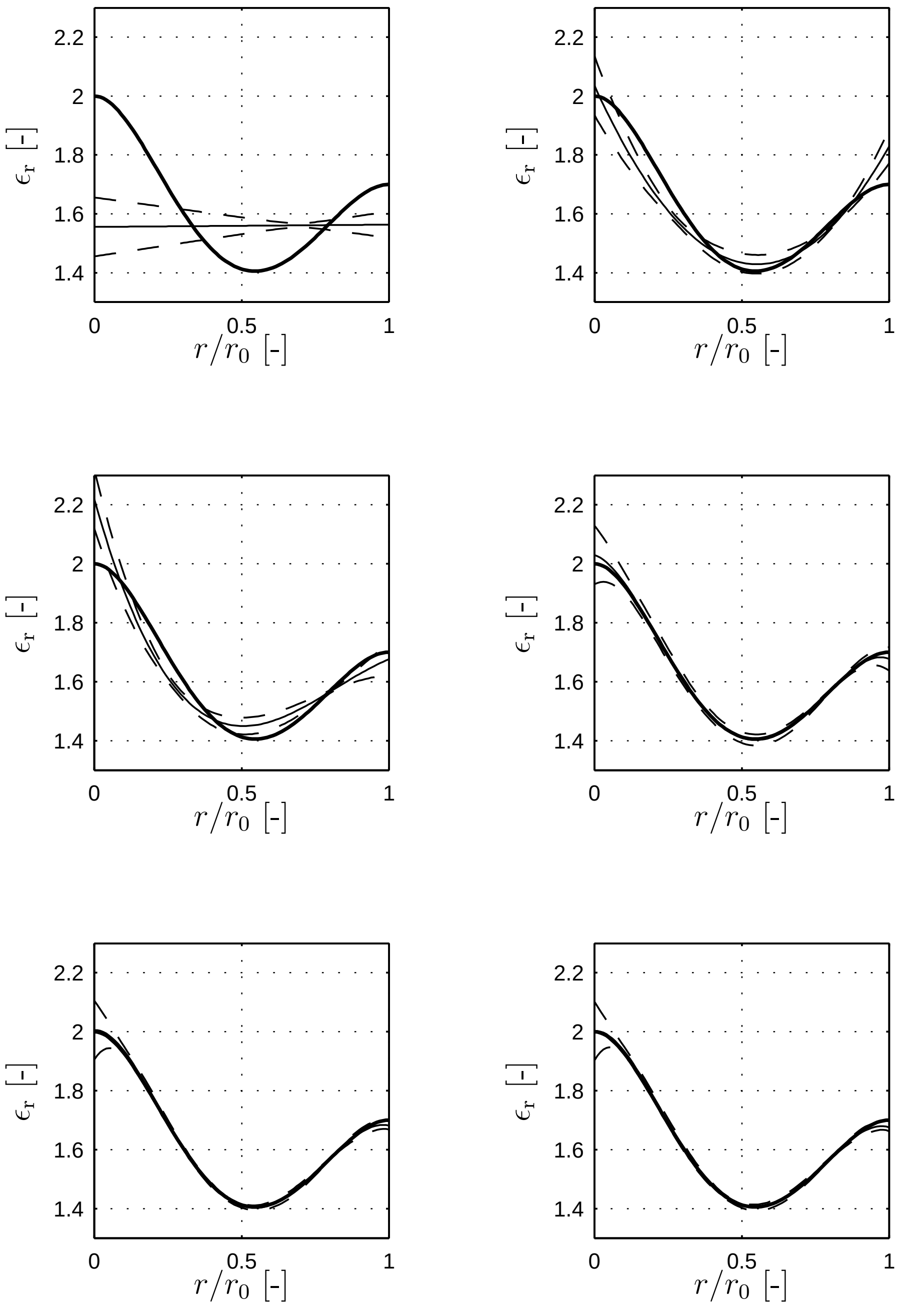

Figure 5: Relative permittivity as a function of radial coordinate for different number of degrees of freedom: $M = 2$ – top-left; $M = 3$ – top-right; $M = 4$ – middle-left; $M = 5$ – middle-right; $M = 6$ – bottom-left; and $M = 7$ – bottom-right. The solid curves show the permittivity $\epsilon_{\mathrm{r}}^{\mathrm{A}}$ (thick curve) and $m_{\epsilon_{\mathrm{r}}} = E[\epsilon_{\mathrm{r}}(r; \hat{\mathbf{a}})]$ (thin curve) while the dashed curves indicate a confidence region normalized to yield a maximum standard deviation of magnitude 1/10.

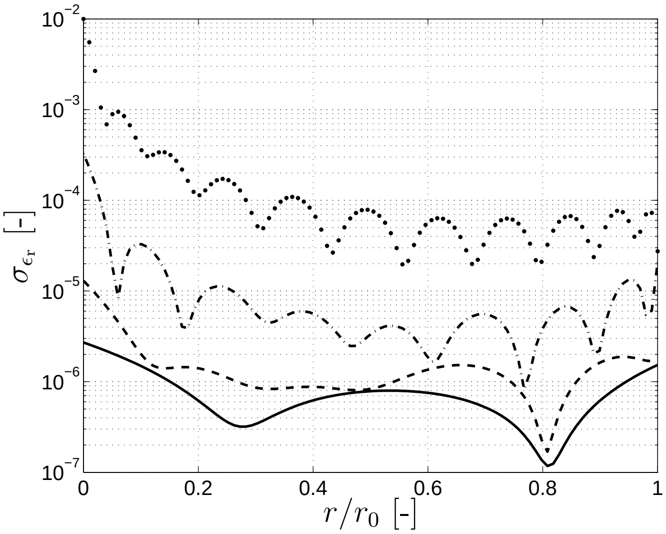

Figure 6: Standard deviation $\sigma_{\epsilon_r}(r)$ for the relative permittivity: $M = 4$ – solid curve; $M = 6$ – dashed curve; $M = 9$ – dash-dotted curve; and $M = 12$ – dotted curve. Here, the SNR is 104 dB.

yields an ill-conditioned problem for large values of M and we find that $M > 20$ cannot give accurate solutions since the problem becomes too ill-conditioned. Currently, we are implementing a parameterization of the permittivity that is based piecewise low-order Bézier curves subject to continuity conditions and our most recent results will be shown at the conference.

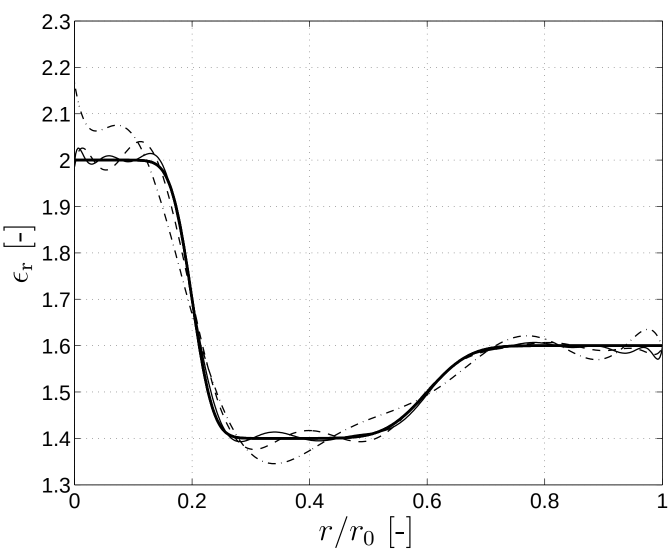

Figure 7: Reconstructed relative permittivity as a function of radial coordinate for different number of degrees of freedom: $M = 10$ – dash-dotted curve; $M = 15$ – dashed curve; and $M = 20$ – solid curve. The thick solid curve shows the permittivity ϵ_r^B subject to reconstruction.

M [-]	SNR [dB]	$\mathcal{E}_{\epsilon_\mathrm{r}^\mathrm{A}}$ [-]
2	5.3	$1.2 \cdot 10^{-1}$
3	18.7	$3.4 \cdot 10^{-2}$
4	19.1	$3.6 \cdot 10^{-2}$
5	23.4	$9.2 \cdot 10^{-3}$
6	32.5	$6.5 \cdot 10^{-3}$
7	33.3	$6.7 \cdot 10^{-3}$
8	38.7	$6.2 \cdot 10^{-3}$
9	60.5	$5.4 \cdot 10^{-3}$
10	77.5	$5.2 \cdot 10^{-3}$
11	85.3	$5.3 \cdot 10^{-3}$
12	90.3	$5.1 \cdot 10^{-3}$

Table 1: SNR required to achieve a maximum standard deviation of 0.05 in the reconstruction together with the corresponding relative error $\mathcal{E}_{\epsilon_\mathrm{r}^\mathrm{A}} = ||\epsilon_\mathrm{r}(r;\mathbf{a}^*) - \epsilon_\mathrm{r}^\mathrm{A}(r)||_2/||\epsilon_\mathrm{r}^\mathrm{A}(r)||_2$ in the L_2-norm.

5.5 Determination of model order

It is challenging to select the number of degrees of freedom M to be used in the parameterization (22) for situations with very limited a priori information about the permittivity profile subject to reconstruction. In practice, we can monitor the value of the goal function (20) as the value for M is incremented. At the point when further increments of M do not yield substantially lower values for the goal function, it may be concluded that a sufficiently high model order is found given the parameterization at hand. Unfortunately, this approach yields no guarantees that the correct permittivity profile has been found, even if the value of the goal function is zero which corresponds to a perfect fit between S_{pq}^C and S_{pq}^M. However, the reconstruction capabilities are in general improved when the number of waveguides is increased and the frequency band is enlarged. We find that extensive computational studies of the type that has been presented in this article can give important information concerning the inverse problem at hand and that this information may be used to design an inverse experiment. In addition, the computational environment can be used for extensive parameter studies that provide information about the reconstruction capabilities: (i) the risk of identifying an incorrect permittivity profile despite a low value of the goal function; (ii) the impact of the parameterization of the material; and (iii) the reconstruction error due to noise and computational errors.

We are currently incorporating model-order selection methods based[21] on the likelihood ratio test, which is used in estimation theory.[22] These methods attempt to find a good balance between two main error contributions. First, the so-called model error is associated with the inability of the parameterization to accurately approximate the permittivity subject to reconstruction. This error contribution can be reduced by increasing the model order. Secondly, a higher model-order yields a larger error due to the presence of measurement noise and this error contribution is basically proportional to the model order. Thus, there is a trade-off point where the total error has a minimum, when it is considered a function of the model order. This effect is clearly visible in Fig. 6, where the standard deviation increases with M.

6 CONCLUSIONS

We present and test a reconstruction algorithm for inverse problems, where Maxwell's equations are solved in a 2D setting. In particular, we consider a model problem that consists of a circular cavity with six parallel-plate waveguides connected to its perimeter. The sensitivity of the scattering parameters with respect to changes in the relative permittivity is formulated in terms of the continuum variables for the transverse magnetic case. We express the sensitivity in terms of the field solution of (i) the original field problem and (ii) an adjoint field problem. Consequently, the gradient can be evaluated as a post-processing step once the scattering matrix and its underlying field solutions have been computed, where the additional computational cost is relatively small and independent of the number of degrees of freedom that are used to parameterize the material distribution subject to reconstruction. This allows for good flexibility in terms of the choice of field solver, since the optimization algorithm is decoupled from the computation of the field solution.

The permittivity distribution subject to reconstruction is parameterized in terms of a set of basis functions and unknown coefficients, where the coefficients are determined by the reconstruction algorithm. We exploit the misfit between the measured and computed scattering matrix, where the goal function is formulated as an average of this difference with respect to a user-specified frequency range and all pairs of available waveguide ports that feature in the scattering matrix. The electromagnetic field problem is solved by the finite element method, where we use Galerkin's method and expand the magnetic field transverse to the cylinder axis in terms of the lowest-order curl-conforming elements on triangles.

We test the reconstruction algorithm on a simple test case, where the permittivity profile subject to reconstruction can be expressed exactly by the parameterization used by the reconstruction algorithm. We find that a resolution of 30 points per wavelength in free-space yields a relative error in the reconstruction of about 1% for a permittivity profile with the relative permittivity in the range $[1.4, 2.0]$. For parameterizations that cannot exactly represent the permittivity profile subject to reconstruction, the reconstructions suffer from an approximation error that stems from the insufficient flexibility in the parameterization. Further, we investigate the impact of noise added to the scattering parameters. In particular, we compute the expected value and standard deviation for the reconstructed permittivity profiles. It is found that as the model order is increased, it is necessary to increase the signal-to-noise ratio in order to maintain a given constant standard deviation for the reconstructed profile.

7 ACKNOWLEDGEMENTS

The authors are grateful for the support from Dr Staffan Folestad and Dr Lubomir Gradinarsky at AstraZeneca, Mölndal, Sweden. Also, the authors thank Professor Anders Rasmuson at the Department of Chemical and Biological Engineering, Chalmers University of Technology for interesting discussions.

REFERENCES

[1] B. Larsson, B. A. Bengtsson, and M. Gustafsson, "Nondestructive detection of decay in living trees," *Tree Physiology*, vol. 24, no. 7, pp. 853–858, 2004.

[2] D. W. Winters, J. D. Shea, P. Kosmas, B. D. Van Veen, and S. C. Hagness, "Three-dimensional microwave breast imaging: Dispersive dielectric properties estimation using patient-specific basis functions," *IEEE Trans. Med. Imag.*, vol. 28, pp. 969–981, July 2009.

[3] K. Harada, Y. Kozima, Y. Fujii, and S. Takeuchi, "Measurements of blast furnace inner-state by magnetometers," *IEEE Trans. Magn.*, vol. MAG-16, pp. 698–700, September 1980.

[4] M. El-Shenawee, O. Dorn, and M. Moscoso, "An adjoint-field technique for shape reconstruction of 3-d penetrable objects immersed in lossy medium," *IEEE Trans. Antennas Propagat.*, vol. 57, pp. 520–534, February 2009.

[5] J. M. Jin, *The Finite Element Method in Electromagnetics (2nd Edition)*. New York, NY: John Wiley & Sons, 2002.

[6] A. Taflove and S. C. Hagness, *Computational Electrodynamics: The Finite-Difference Time-Domain Method (3rd Edition)*. Boston, MA: Artech House, 2005.

[7] A. N. Tikhonov and V. Y. Arsenin, *Solutions to ill-posed problems*. New York, NY: Winston-Wiley, 1977.

[8] M. Gustafsson, *Wave splitting in direct and inverse scattering problems*. Ph.D. dissertation, Lund University of Technology, 2000.

[9] M. Gustafsson and S. He, "An optimization approach to two-dimensional time domain electromagnetic inverse problems," *Radio Science*, vol. 35, pp. 525–536, March-April 2000.

[10] O. Pironneau, *Optimal shape design for elliptic systems*. New York, NY: Springer, 1984.

[11] J. R. Shewchuk, "Triangle: Engineering a 2D Quality Mesh Generator and Delaunay Triangulator," in *Applied Computational Geometry: Towards Geometric Engineering* (M. C. Lin and D. Manocha, eds.), vol. 1148 of *Lecture Notes in Computer Science*, pp. 203–222, Springer-Verlag, 1996. From the First ACM Workshop on Applied Computational Geometry.

[12] J. C. Nédélec, "Mixed finite elements in $\mathbb{R}^3$," *Numer. Math.*, vol. 35, no. 3, pp. 315–341, 1980.

[13] D. M. Pozar, *Microwave engineering.* New York, NY: Wiley, 1998.

[14] A. Bondeson, Y. Yang, and P. Weinerfelt, "Shape optimization for radar cross sections by a gradient method," *Int. J. Numer. Meth. Engng.*, vol. 61, pp. 687–715, October 2004.

[15] Y. Yang, T. Halleröd, D. Ericsson, A. Hellervik, A. Bondeson, and T. Rylander, "Gradient optimization of microwave devices using continuum design sensitivities from the adjoint problem," *IEEE Trans. Magn.*, vol. 41, pp. 1780–1783, May 2005.

[16] T. Rylander, P. Hashemzadeh, and M. Viberg, "Reconstruction of metal protrusion on flat ground plane," *accepted for publication in IET Microw. Antennas Propag.*, 2010.

[17] K. Holmström, A. O. Göran, and M. M. Edvall, *USER'S GUIDE FOR TOMLAB 7.* Tomlab Optimization AB, Västerås Technology Park, Trefasgatan 4, SE-72130 Västerås, Sweden, 2009.

[18] A. Bondeson, T. Rylander, and P. Ingelström, *Computational Electromagnetics.* Berlin: Springer, 2005.

[19] J. C. Ye, Y. Bresler, and P. Moulin, "Cramér-Rao bounds for 2-D target shape estimation in nonlinear inverse scattering problems with application to passive radar," *IEEE Trans. Antennas Propagat.*, vol. 49, pp. 771–783, May 2001.

[20] J. C. Ye, Y. Bresler, and P. Moulin, "Cramér-Rao bounds for parameteric shape estimation in inverse problems," *IEEE Trans. Image Processing*, vol. 12, pp. 71–84, January 2003.

[21] P. Stoica and Y. Selén, "Model order selection – a review of information criterion rules," *IEEE Signal Processing Mag.*, vol. 21, pp. 36–47, July 2004.

[22] S. M. Kay, *FUNDAMENTALS OF STATISTICAL SIGNAL PROCESSING - ESTIMATION THEORY.* Englewood Cliffs, NJ: Prentice-Hall, 1993.